SUPPLEMENTAL FIGURES AND LEGENDS

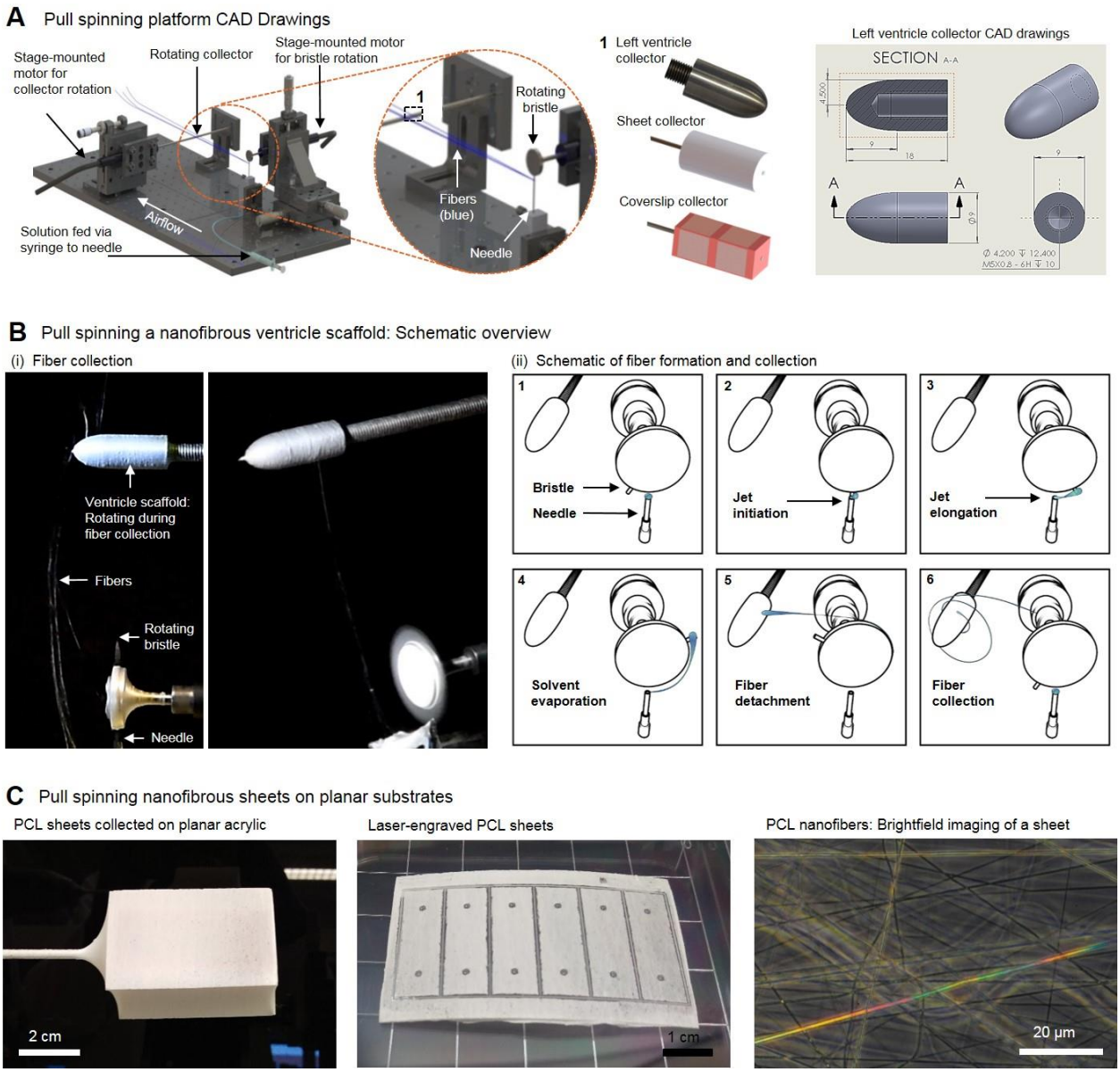

Figure S1. Nanofiber production by pull-spinning. (A) CAD drawings of a pull spinning system showing ventricle, sheet, and coverslip fiber collectors. (B) Fiber collection on a left-ventricle-shaped ellipsoidal collection mandrel (i) and schematic overview of the pull-spinning process (ii): A rotating bristle dips and pulls a polymer solution that is extruded from a needle (1, 2); jet elongation (3) and solvent evaporation (4) produce fibers (5) that are collected on a rotating ellipsoidal collection mandrel (6). (C) Anisotropic fiber collection on planar substrates and subsequent patterning by laser engraving.

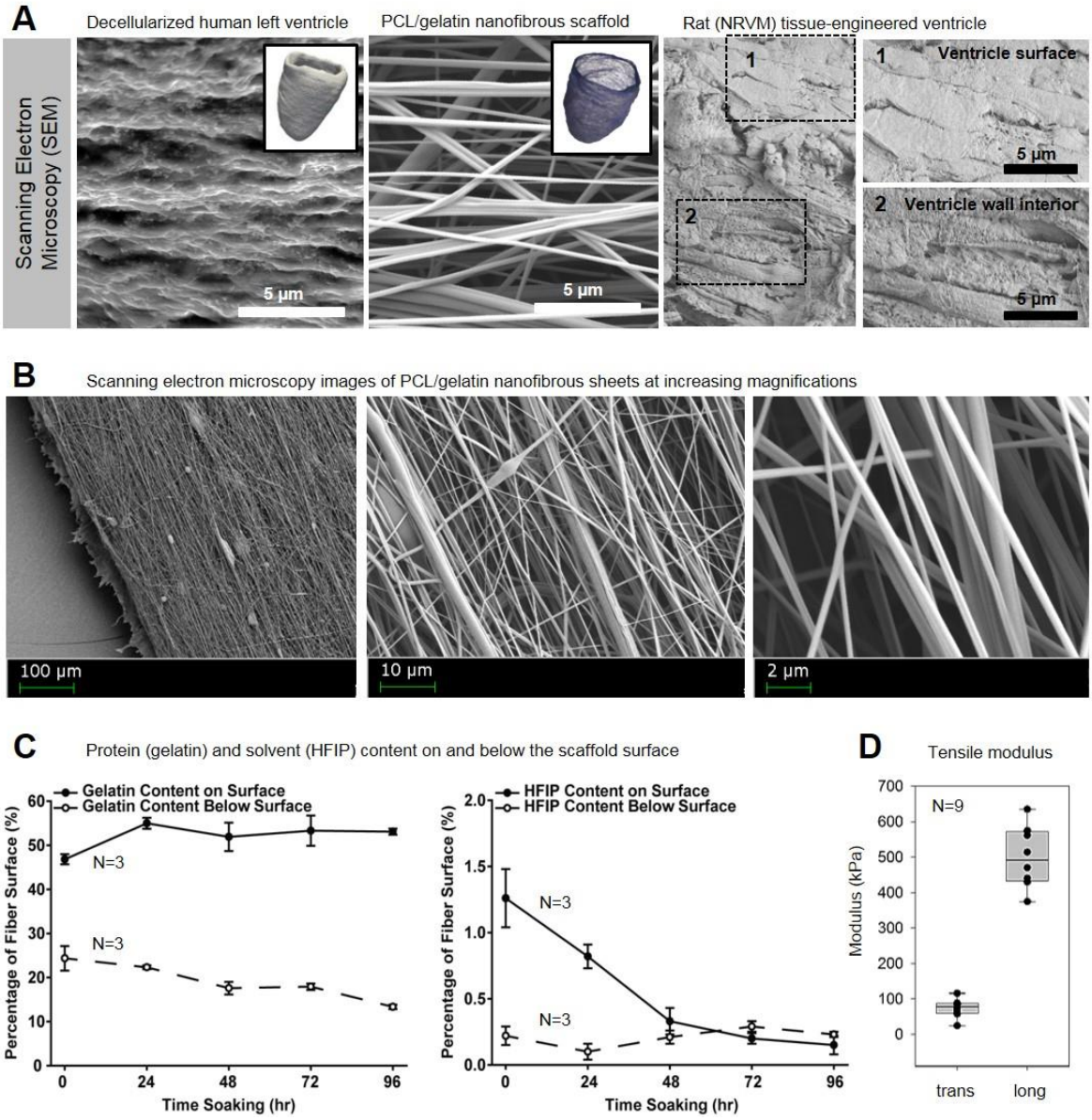

Figure S2. Polymer-protein nanofiber ultrastructure and biochemistry. (A) Scanning electron microscopy (SEM) images comparing ultrastructural features of decellularized human left ventricle myocardial tissue (left) and pull-spun nanofibrous scaffolds before (middle) and after (right) culture with cardiomyocytes. (B) SEM images of PCL/gelatin nanofibrous sheets at increasing magnifications. Sheets were pull-spun using 75/25 PCL/gelatin mixtures diluted to 6% in solvent, bristle rotation rate was 30,000 RPM, collector rotation rate was 300 RPM, feed rate was 0.2 mL/minute, and collector distance was 20 cm. (C) X-ray photoelectron spectroscopy analysis of gelatin and solvent content in PCL/gelatin scaffolds. Estimated percentage gelatin (left) and solvent (right) content in polycaprolactone/gelatin nanofibrous scaffolds after soaking in de-ionized water for up to 96 hours. All values are mean ±s.e.m (N=3). (D) Bi-axial tensile elastic moduli of anisotropic PCL/gelatin scaffolds measured longitudinally (in the direction parallel to the fiber axis), EL = 499.7 ± 30.7 kPa (mean ±s.e.m), or transverse (in the direction perpendicular to the fiber axis), ET = 73.8 ± 9.5 kPa (mean ±s.e.m, N=9). Data are presented as box plots with individual data points overlaid, where lower or upper edges of the box represent 25th or 75th percentiles, the middle bar is the median, and whiskers are minimum and maximum values.

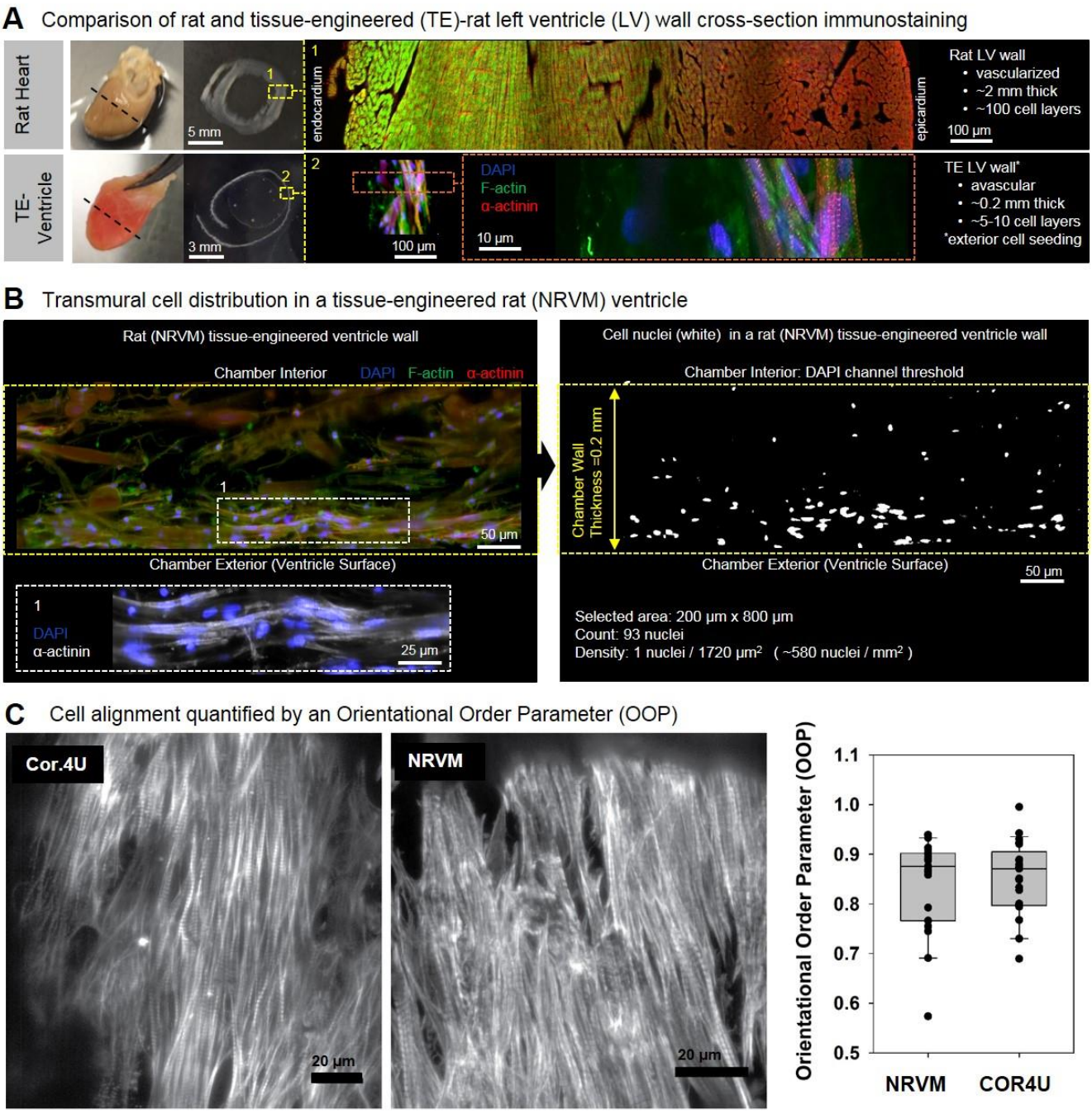

Figure S3. Analysis of cardiomyocyte distribution and alignment in ventricle scaffolds. (A) Comparison of an adult rat left ventricular wall cross-section (top) and a thin-walled tissue-engineered NRVM ventricle wall cross-section (bottom). (B) Transmural cell distribution in a tissue-engineered NRVM ventricle that was seeded via the exterior surface. DAPI channel thresholding and nuclei counts provided a cell density estimate of ~580 cells/mm^2 with a higher density near the ventricle's exterior surface. (C) Cell alignment quantified by orientational order parameter (OOP) that ranges from zero (random organization) to one (perfect alignment). Immunostained F-actin were analyzed for OOP. Values of 0.85 ± 0.015 (mean ± s.e.m., N = 4 Cor.4U ventricles, 25 fields of view) and 0.084 ± 0.022 (mean ± s.e.m. N = 2 NRVM ventricles, 19 fields of view) indicated near-perfect alignment. Data are presented as box plots with individual data points overlaid, where lower or upper edges of the box represent 25th or 75th percentiles, the middle bar is the median, and whiskers are 10th and 90th percentiles.

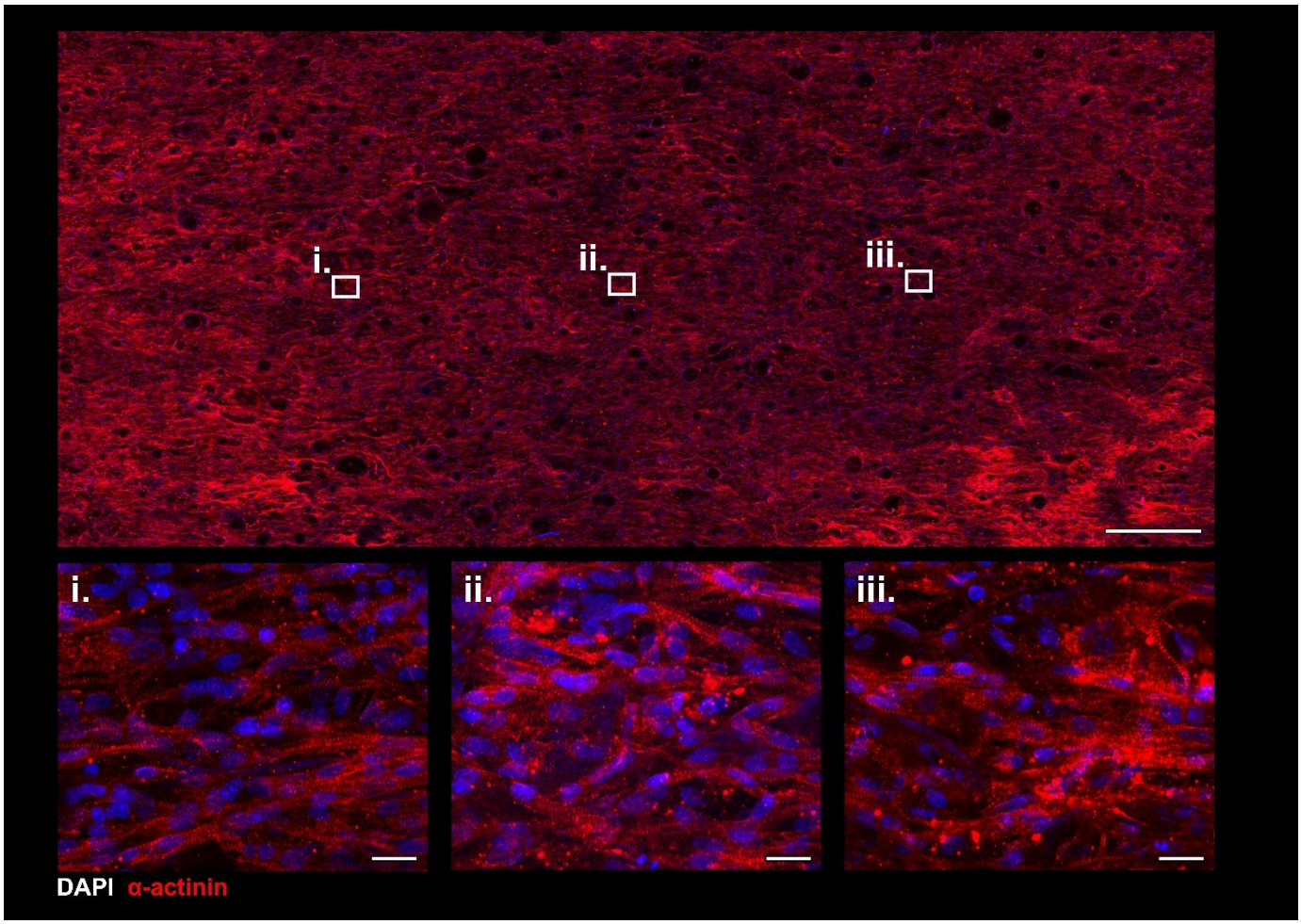

Figure S4. Confocal fluorescent tile scan projection of a neonatal rat ventricular myocyte ventricle following 12 days in culture, reconstructed using pairwise matching (upper, standard deviation projection, scale bar 1mm), showing long range tissue organization and coverage, with the corresponding high magnification insets taken from the pre-determined highlighted regions (lower, scale bars, 20μm).

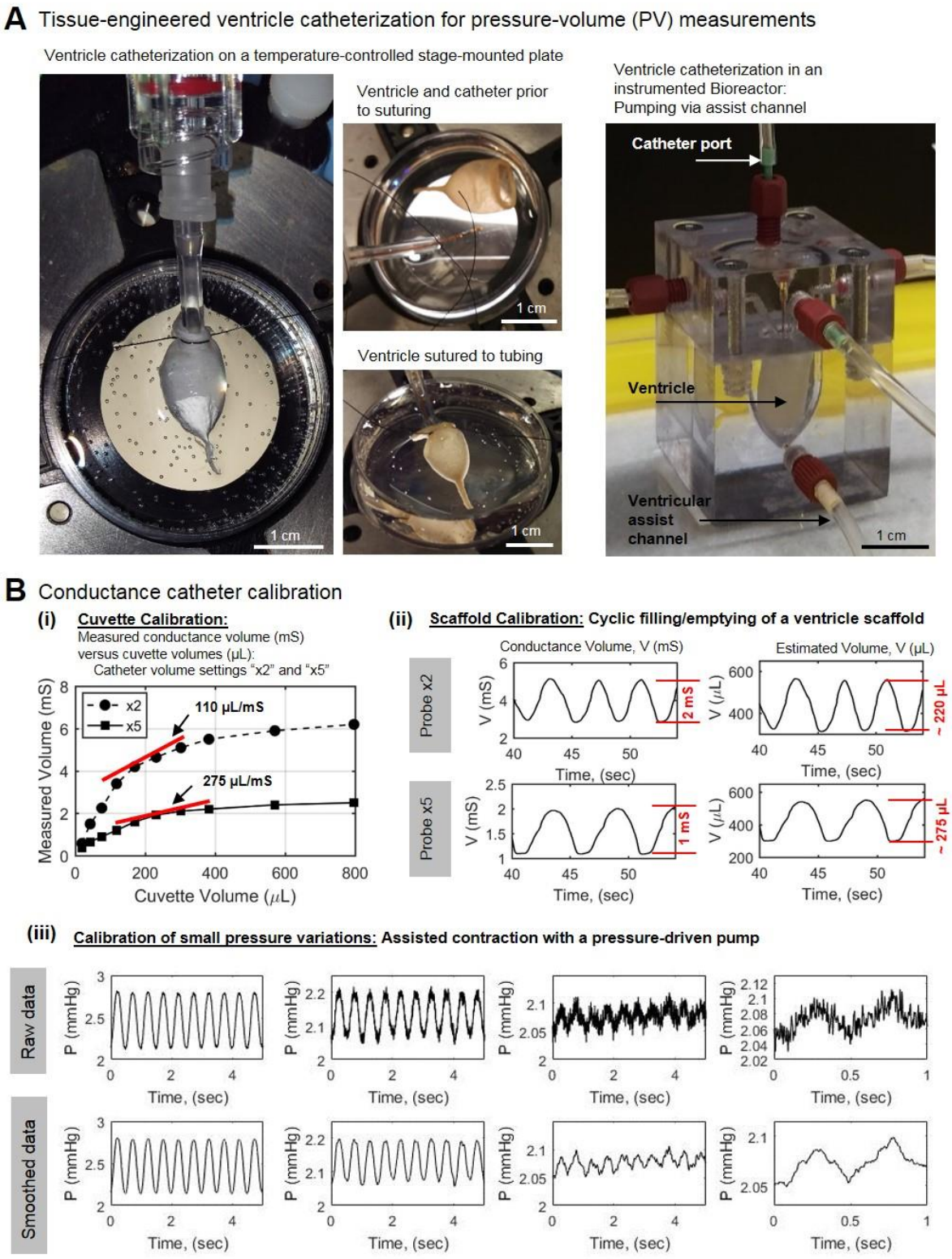

Figure S5. Pressure-volume measurements obtained by tissue-engineered ventricle catheterization. (A) Experimental setups for ventricle catheterization in a temperature-controlled bath. (B) Conductance volume catheter calibration using manufacturer-supplied cuvettes (i) and by manual inflation/deflation of catheterized cell-free scaffolds (ii). Small-amplitude pressure recordings (iii) were obtained by assisted ventricle scaffold contraction using our instrumented bioreactor's ventricular assist channel and pressure supplied by a programmable pressure-driven microfluidic pump.

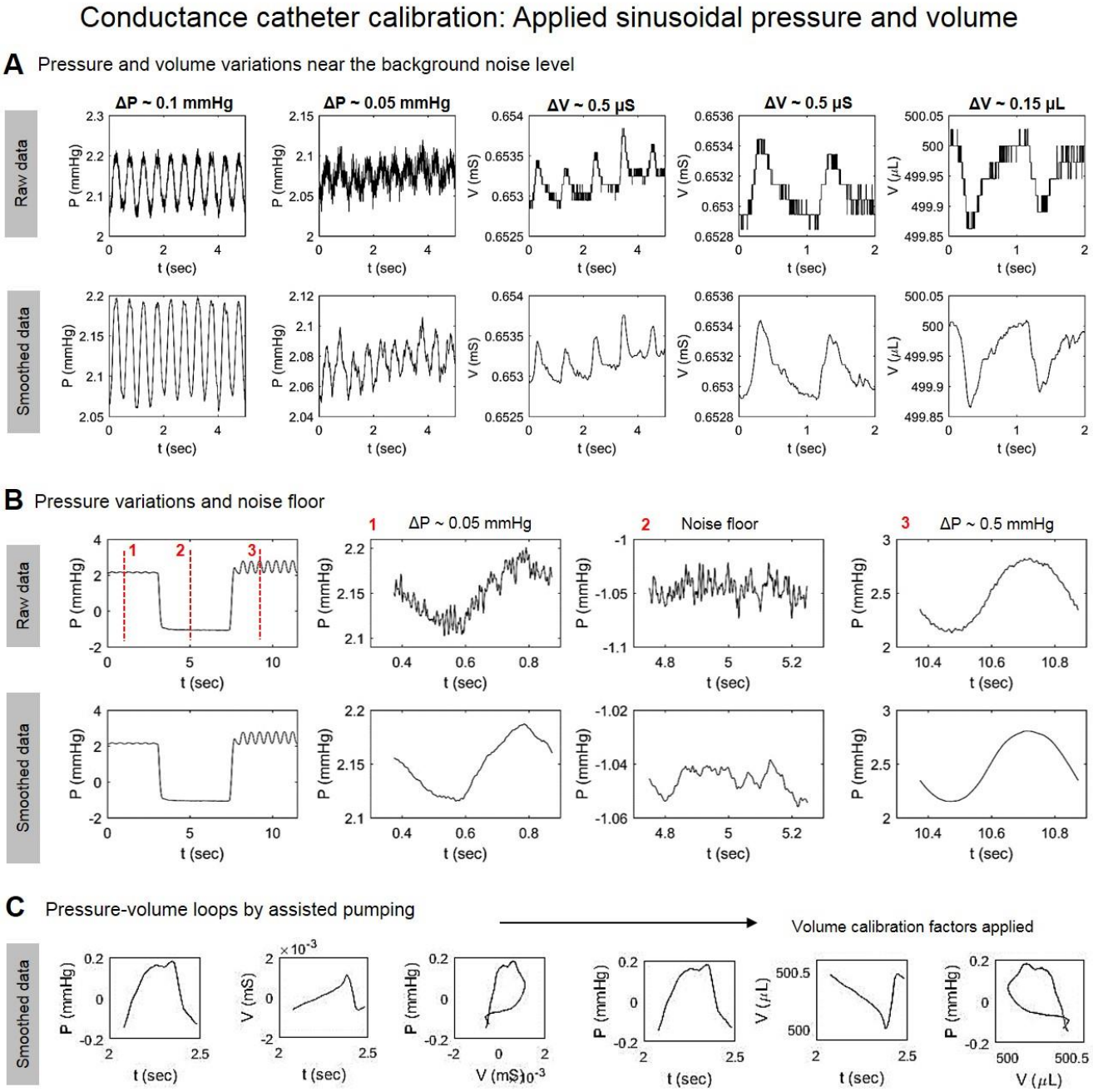

Figure S6. Small-amplitude pressure, P, and volume, V, calibration. P and V were measured during assisted ventricle scaffold contraction using our instrumented bioreactor's ventricular assist channel and pressure supplied by a programmable pressure-driven microfluidic pump. (A) Cyclic loading with ΔP and ΔV values comparable to those expected to be generated by our tissue engineered ventricle chambers (ΔP ~0.05 mmHg, ΔV ~1 µL). (B) Sinusoidal pressure variations of two different amplitudes (peak-to peak ΔP = 0.05 mmHg in region "1" or ΔP = 0.5 mmHg in region "3"), compared with signal noise when no external pressure was applied (region "2"). (C) P-V recordings and loops before and after application of volume calibration factors.

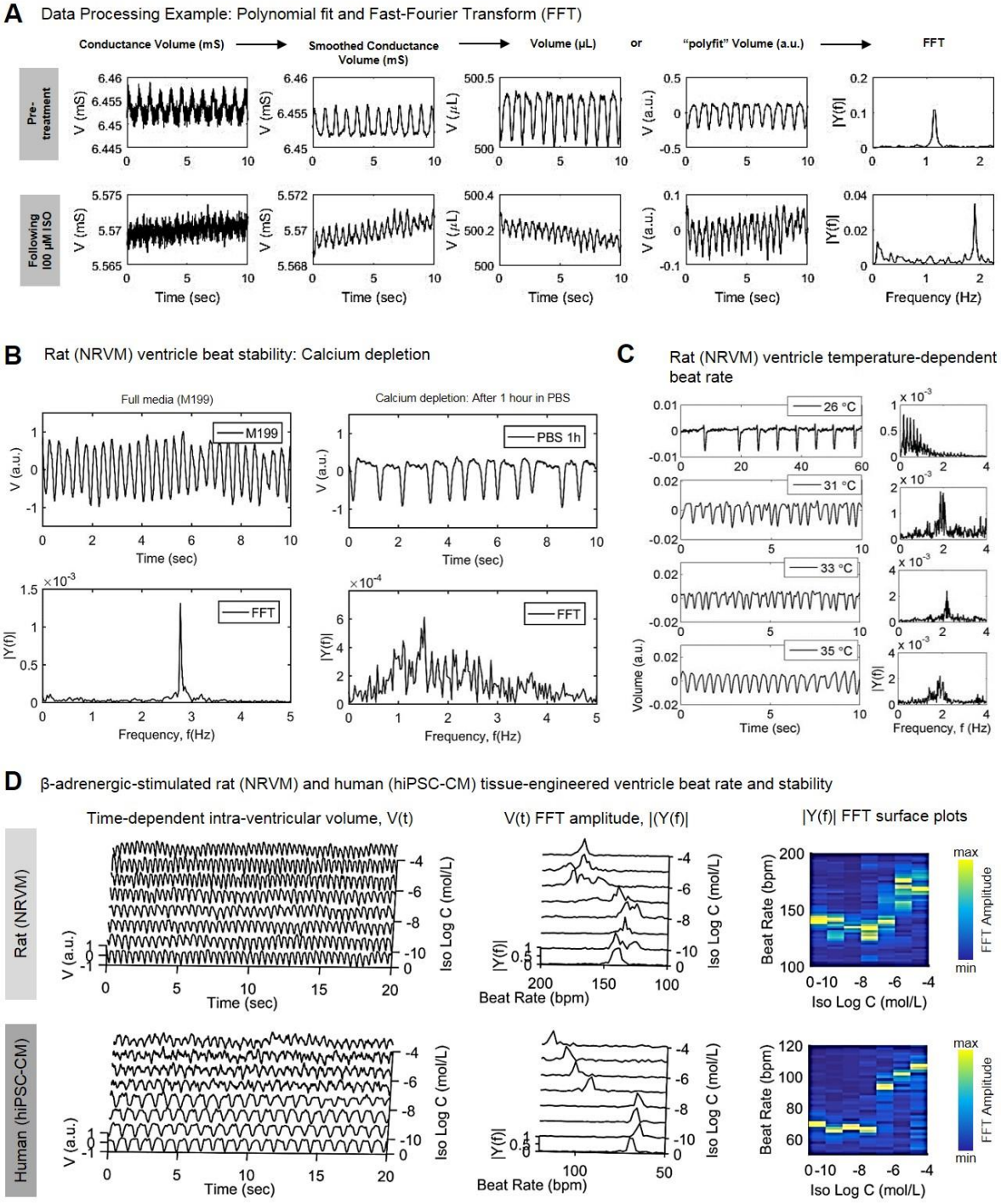

Figure S7. Time and frequency domain analysis of tissue-engineered ventricle beat rates. (A) Example data processing steps include data smoothing, application of conductance volume calibration factors, polynomial fits to remove signal drift, and Fourier-transformation to produce frequency spectra of ventricle beat rates over defined time intervals. (B) Effects of calcium depletion on neonatal rat ventricular myocyte (NRVM) ventricle beat rate. Stable beat rates observed in full culture media (M199) gave way to broad beat rate distributions in calcium-depleted phosphate-buffered saline (PBS). We note that sustained contraction that we observed following 1 hour in PBS is not compatible with natural heart muscle, which cannot contract under these conditions, and we speculate that the residual contractions were caused by very low concentrations of calcium ions trapped in the scaffold bed and/or in the experimental apparatus. (C) Temperature-dependence of NRVM ventricle beat rate. Low beat rates on the order of ~0.1 Hz observed in room-temperature Tyrode's solution (top panel) increased to ~2 Hz for temperatures between ~30 ºC and ~35 ºC. (D) Time- and frequency-domain plots of rat and human tissue-engineered ventricle beat rates in response to isoproterenol stimulation. Volume data (left) were Fourier-transformed to produce single-sided amplitude spectra, |Y(f)|, representing beat rate

distributions (middle). Surface plots of |Y(f)| produced beat rate heat maps (right) showing beat rate and stability over a given time period (20 seconds in this case).

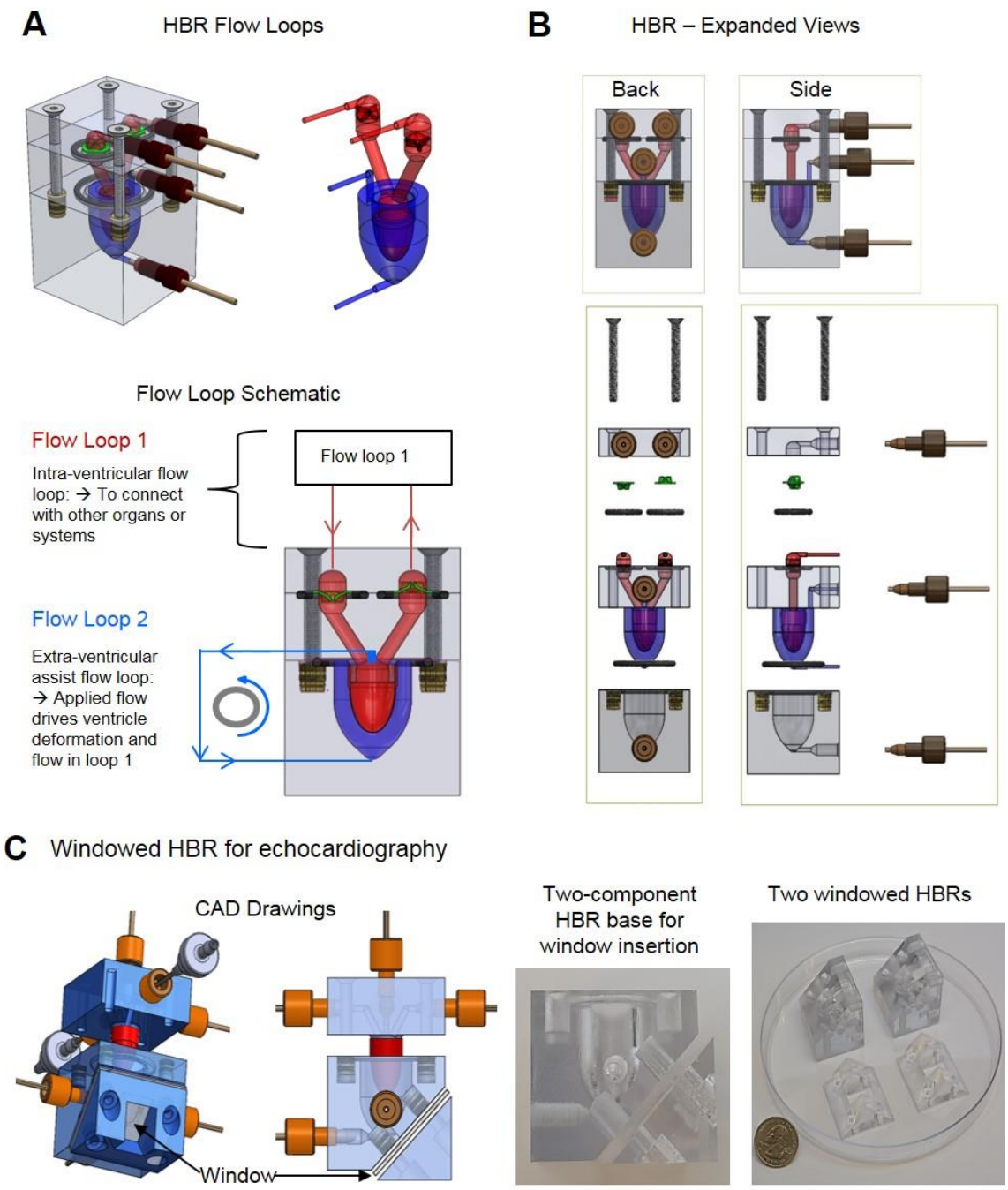

Figure S8. Heart bioreactor (HBR) computer-aided design (CAD) drawings. (A) Inter- or intra- ventricular flow loops are shown in red or blue, respectively. External pressure supplied via the extra-ventricular flow loop drives ventricle contraction (i.e., ventricular assist), which drives fluid flow through the intraventricular flow loop. (B) Expanded view of the HBR showing components and assembly. (C) CAD drawings and photos of an HBR variant, modified for modular placement of observation window materials. We used silicone window inserts for observation by ultrasound.

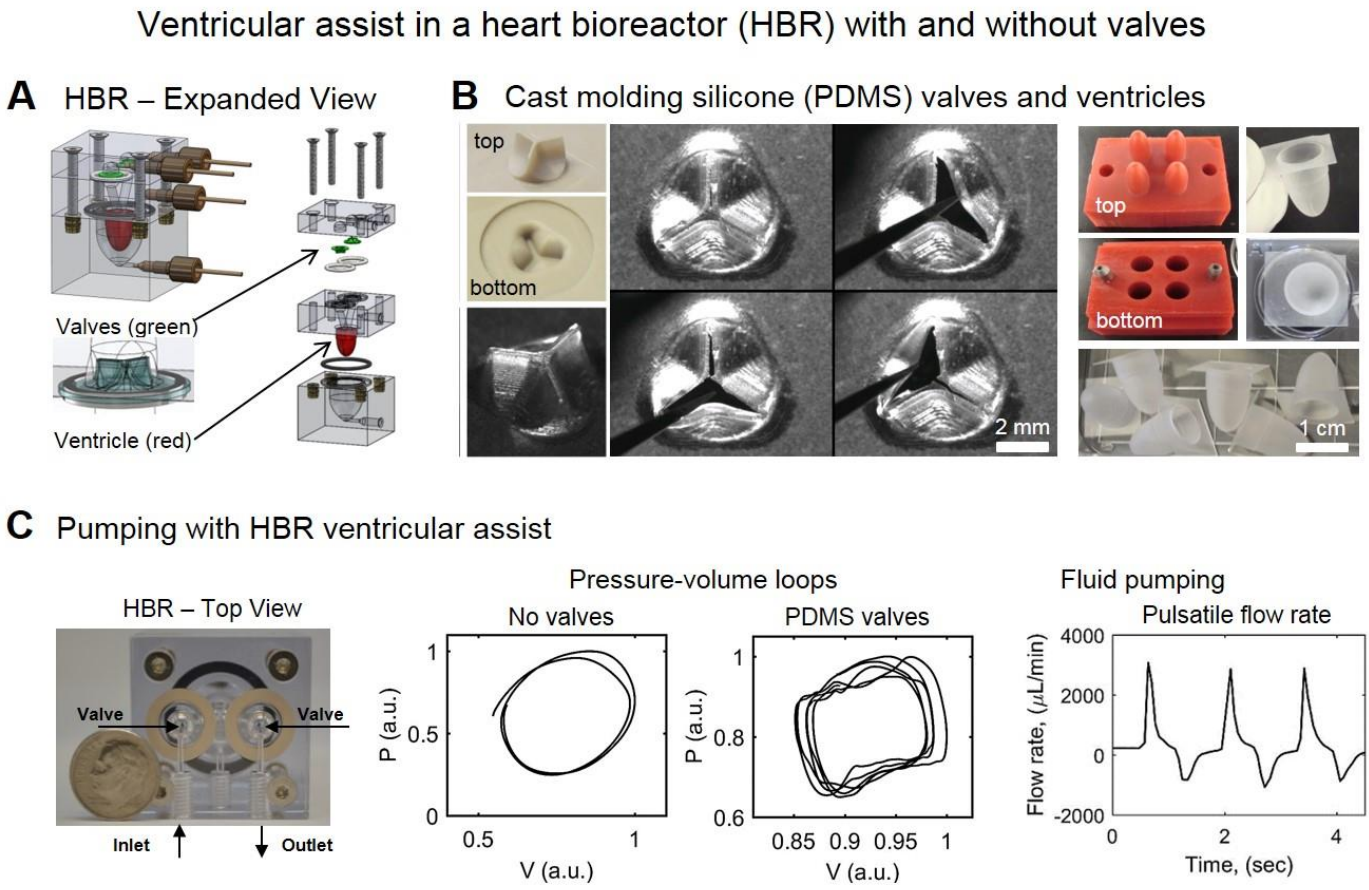

Figure S9. Heart Bioreactor (HBR) components and assembly. (A) Computer-aided design (CAD) drawing showing an expanded view of the HBR with valve and ventricle placement indicated. (B) Cast-molding of silicone tricuspid valves and ventricle chambers. The cast-molding procedure produces optional valve or ventricle components that can be assembled within the HBR to support tissue-engineered ventricle assisted contraction and fluid pumping. (C) Pumping by HBR-driven contraction of a cell-free ventricle scaffold: HBR top view (left) shows valve placement and intra-ventricular flow loop inlet and outlets. Pressure-volume loops (middle) acquired without valves are elliptical whereas those acquired with valves show characteristics of functional chamber valves required to direct fluid flow (right).

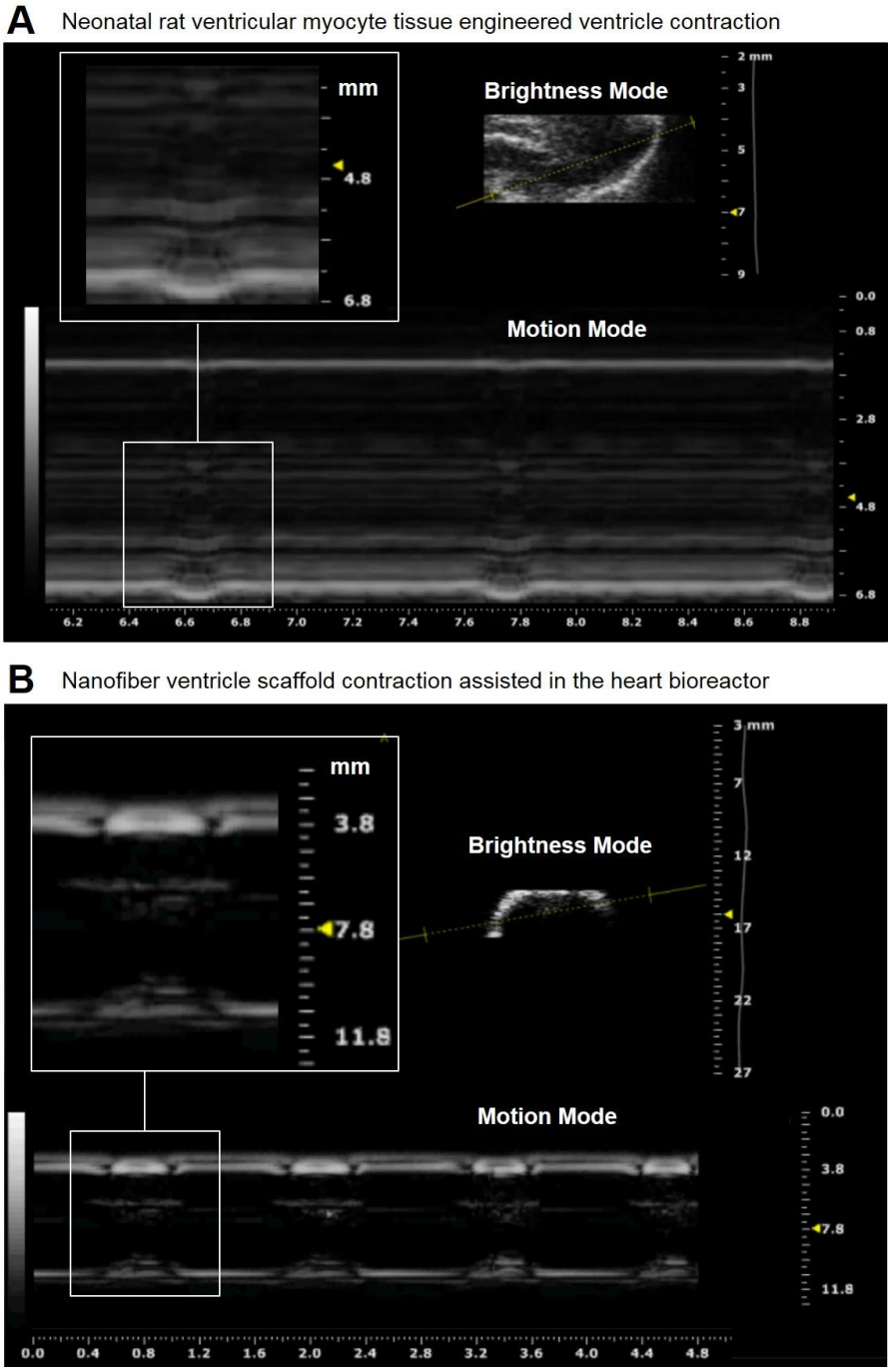

Figure S10. Echocardiographic measurement of a tissue-engineered rat (neonatal ventricular myocytes, NRVM) model ventricle contracting unassisted (A) and a cell-free ventricle scaffold contracting by HBR assist (B). In both cases, cross-sections (brightness mode) and time-dependent traces of the ventricle wall (motion, M-mode) are shown. Insets show magnified views of contractions observed in M-mode. The NRVM model ventricle was imaged on day 14.

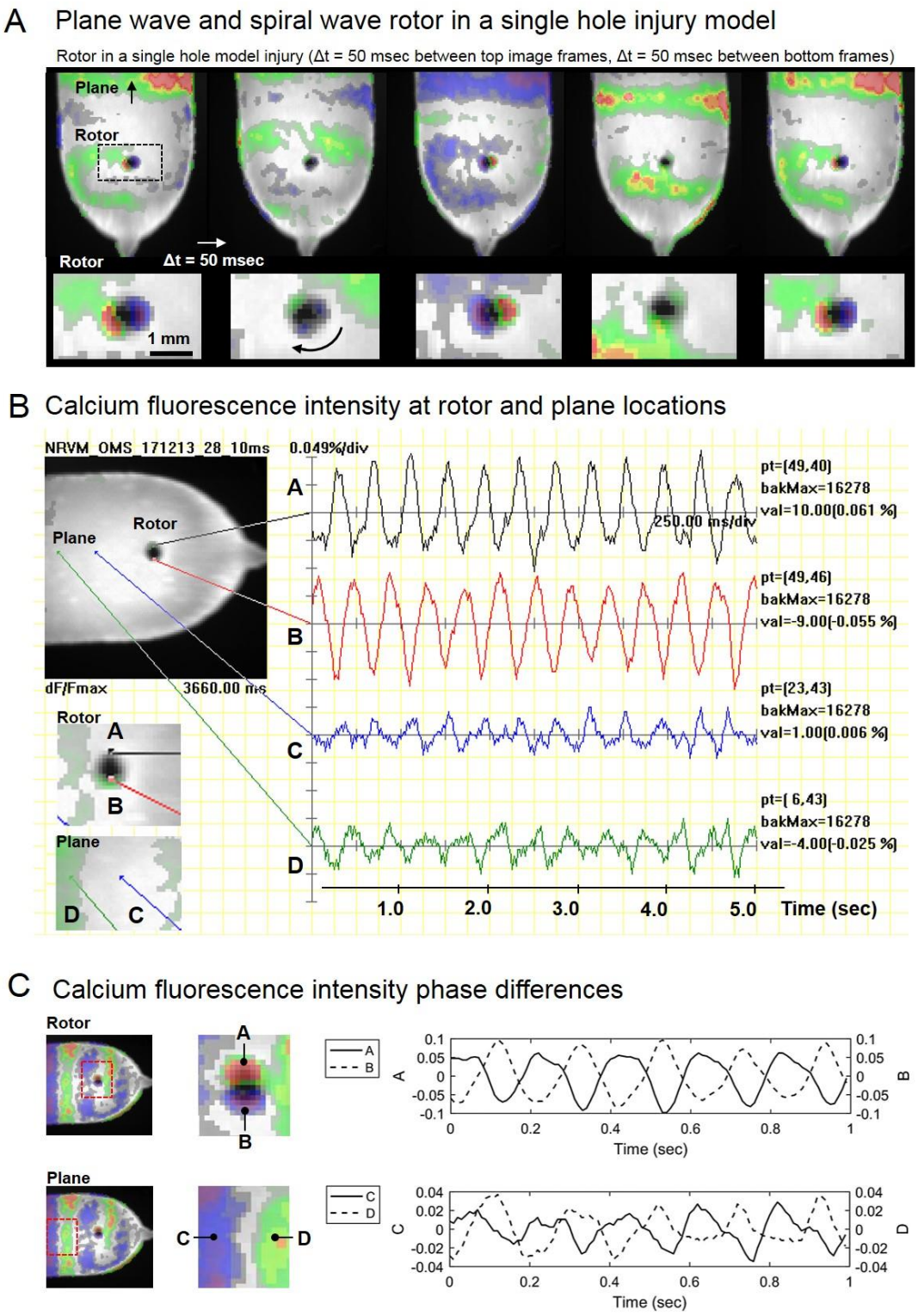

Figure S11. Structural arrhythmia disease model. (A) Calcium wavefront propagation on a model ventricle chamber with single hole anatomical injury. Image frames from left to right show a single rotation of a spiral wave pinned at the defect site, and the propagation of plane waves from the spiral arm towards the ventricle base. (B) Calcium fluorescence intensity measurements near the rotor poles and plane wave peak/trough locations. (C) Co-plots of calcium fluorescence intensity at locations of rotor and plane wave phase differences. The cardiomyocytes were neonatal rat ventricular myocytes (NRVM) and calcium imaging was performed on day 12.

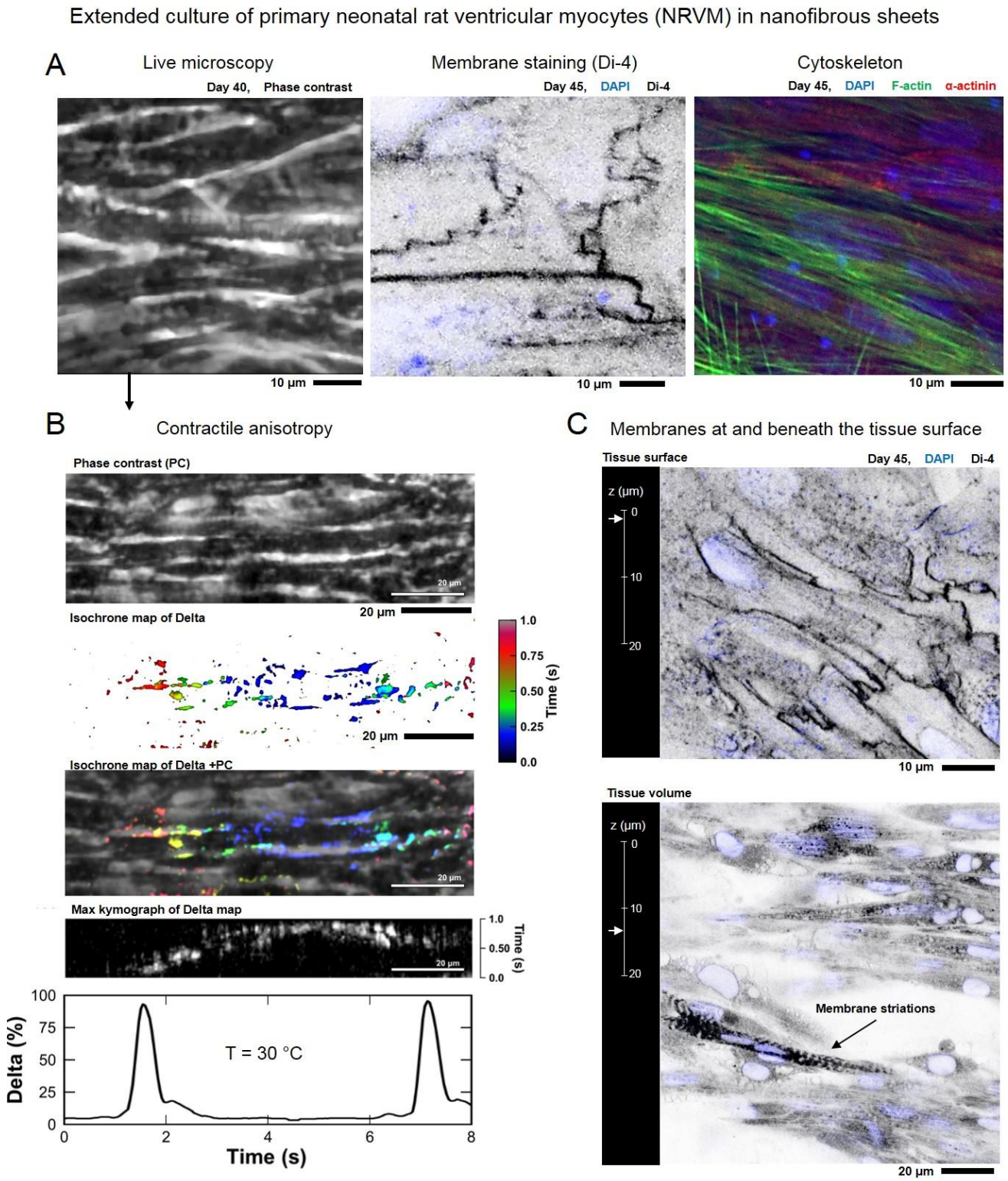

Figure S12 Extended culture (40-45 days) of neonatal rat ventricular myocytes (NRVM) in nanofibrous polycaprolactone/gelatin sheets. Compact anisotropic tissues were observed by light microscopy, membrane and cytoskeletal staining (A), contractile anisotropy was confirmed by mapping the displacement tracked within video recordings (B), and compact tissue structure beneath the tissue surface was observed in confocal microscopy image stack reconstructions of membrane stains (C).

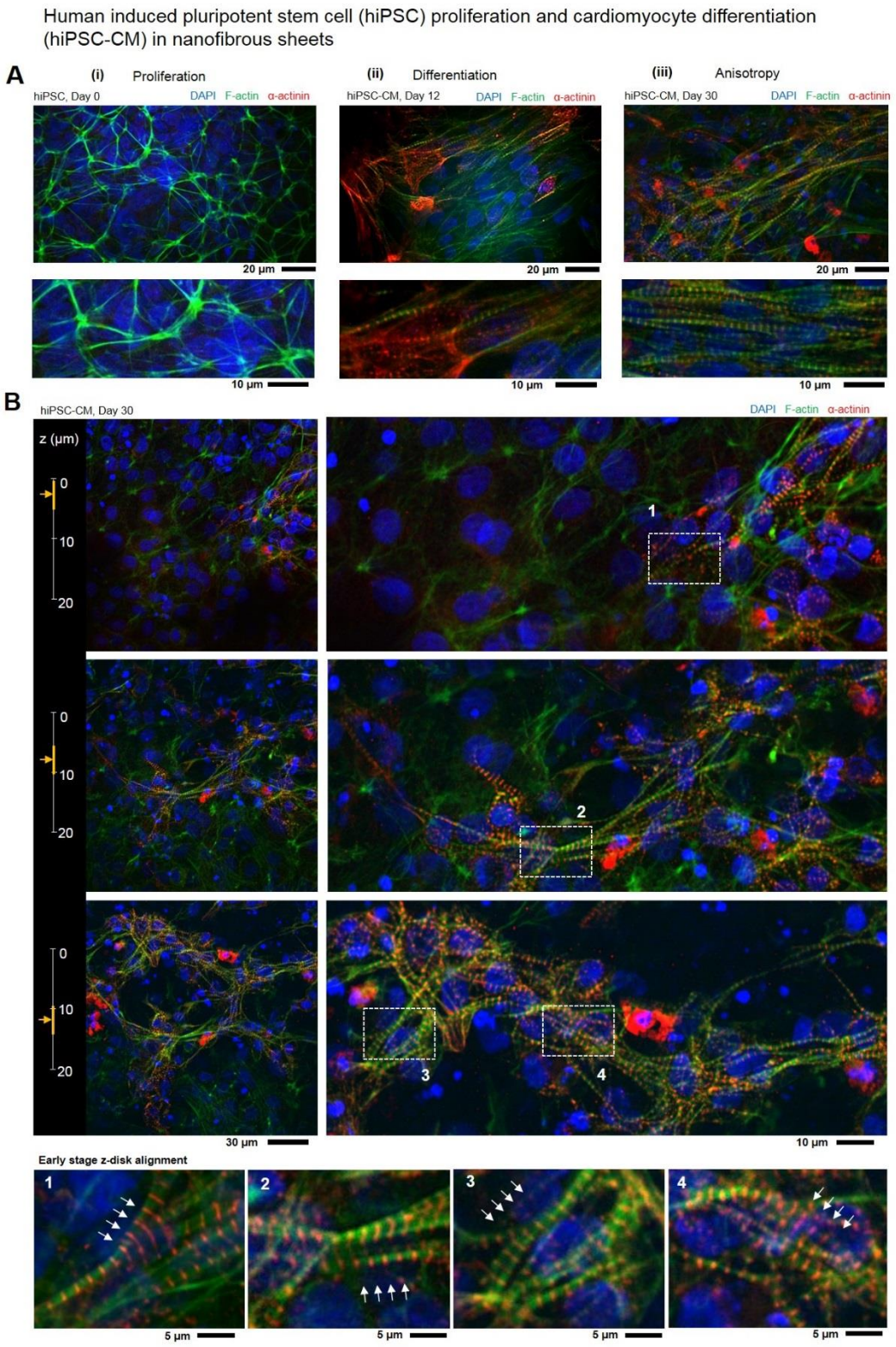

Figure S13. Proliferation of human induced pluripotent stem cells (hiPSC) and in situ differentiation of hiPSC-cardiomyocytes (hiPSC-CM). (A) Human iPSC line PGP1-iPSC seeded at a density of 10^5 cells/cm^2 on the surface of nanofibrous polycaprolactone/gelatin sheets proliferated to confluence following 4 days of culture (i), at which point (day 0) media was changed to induce differentiation. Contraction was observed following ~8-12 days of differentiation, concomitant with early stage sarcomeric expression and assembly observed by immunostaining (ii). Contractile synchrony increased during extended culture periods (30 days), concomitant with anisotropic sarcomeric assembly (iii). (B) Confocal fluorescence microscopy image stack reconstruction at various tissue depths showed hiPSC-CM infiltration of the scaffold and early stages of sarcomeric z-disk alignment.

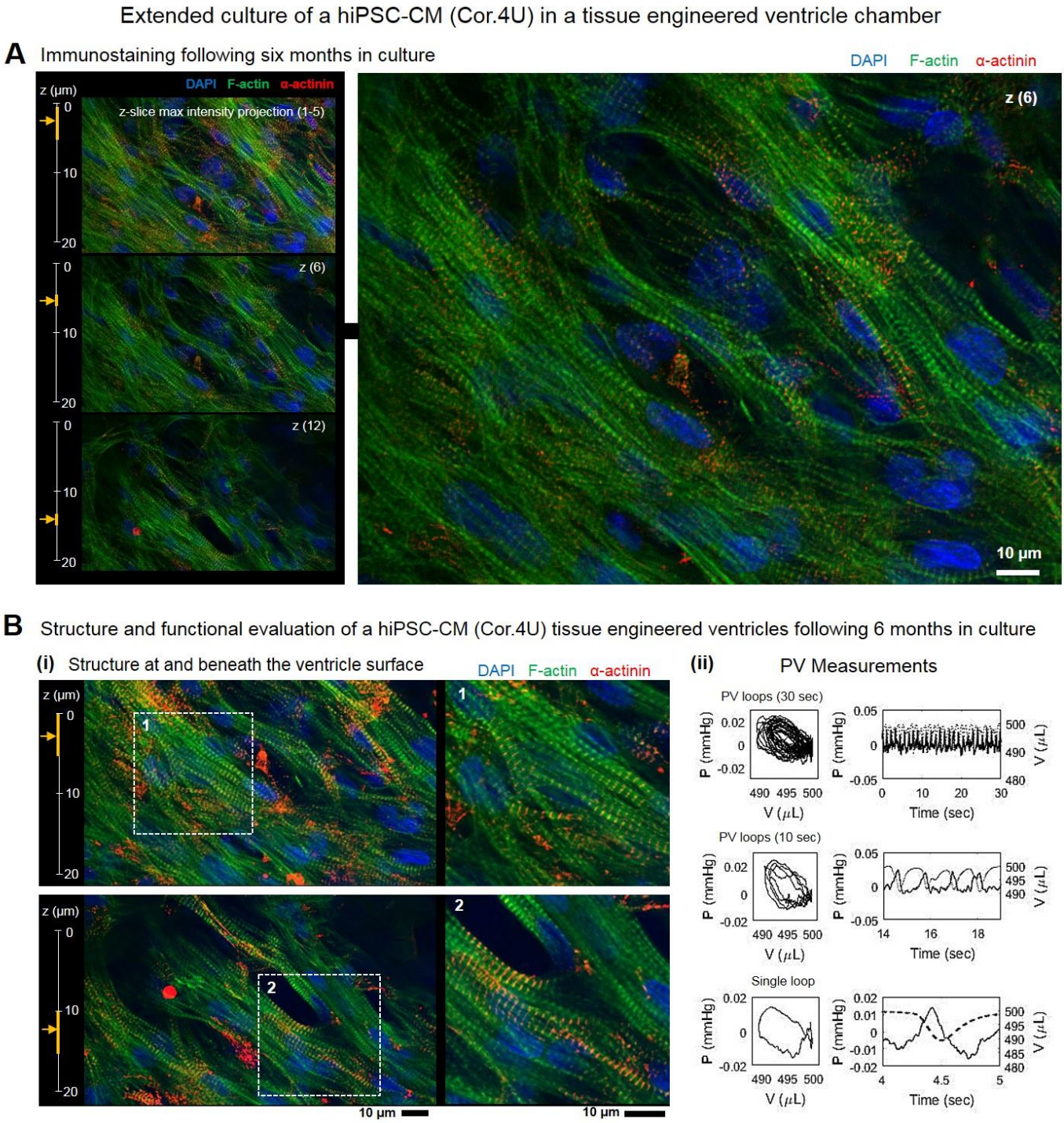

Figure S14. Extended (6-month) culture of human induced pluripotent stem cell-derived cardiomyocytes (hiPSC-CM type: Cor.4U) in a tissue engineered model ventricle chamber. (A) Confocal fluorescence microscopy image stack reconstruction at various tissue depths. (B) Structural and functional characteristics of hiPSC-CM model ventricle following 6 months in culture include compact tissue with extensive z-disk alignment (i) and stable spontaneous contraction enabling continuous pressure-volume recordings (ii).

LEGENDS FOR SUPPLEMENTAL MOVIES

Movie S1, Pull-spinning a nanofibrous ventricle scaffold. A polymer solution fed through a needle is pulled into a fiber by a high-speed rotating bristle. Fiber formation results from jet elongation and solvent evaporation and fibers are collected on a rotating ellipsoidal ventricle scaffold collector.

Movie S2, Micro-computed tomography reconstruction of a nanofibrous ventricle scaffold showing scaffold rotation (left) and cross-sectional reconstruction (right). The length of the ventricle from base to apex is 1 cm and the diameter at the base is 9 mm.

Movie S3, Spontaneous contraction of a plated neonatal rat ventricular myocyte tissue-engineered ventricle. The length of the ventricle from base to apex is 1 cm and the diameter at the base is 9 mm. Culture day is 14.

Movie S4, Magnified views of spontaneously contracting tissue-engineered ventricles, observed using an inverted microscope (brightfield, with a 10X objective). Top panels show ventricle contraction at the surface and bottom panels show contraction near ventricle edges. Scale bars are 0.2 mm. Culture day is 14.

Movie S5, Spontaneously contracting, sutured and catheterized neonatal rat ventricular myocyte tissue-engineered ventricle. Culture day is 14.

Movie S6, Calcium propagation on a neonatal rat ventricular myocyte tissue-engineered ventricle. The white banding structure spanning the ventricle surface from left to right is a topographical feature of the fibrous scaffold. The length of the ventricle from base to apex is 1 cm and the diameter at the base is 9 mm. Pacing frequency was 1 Hz. Culture day is 14.

Movie S7, Calcium propagation on a human induced pluripotent stem cell-derived cardiomyocyte tissue-engineered ventricle surface. The length of the ventricle from base to apex is 1 cm and the diameter at the base is 9 mm. Pacing frequency was 3 Hz. Culture day is 14.

Movie S8, Immunostained human induced pluripotent stem cell-derived cardiomyocytes (Cor.4U type) in a PCL-gelatin nanofiber ventricle scaffold. Culture day is 14. Dimensions are 100 × 50 × 12.4 μm (31 z-slices, 0.40 μm each, interpolated). Immunostains are f-actin (green), α-actinin (red), and DAPI (blue).

Movie S9, Heart Bioreactor (HBR) computer-aided design drawings, including HBR rotation and an exploded view of HBR components.

Movie S10, Echocardiographic imaging of a spontaneously beating neonatal rat ventricular myocyte tissue-engineered ventricle. Culture day is 14.

Movie S11, Echocardiographic imaging of a ventricle scaffold for which contraction was driven by the heart bioreactor.

Movie S12, Calcium propagation on a neonatal rat ventricular myocyte tissue-engineered ventricle before and after injury with a 1-mm diameter biopsy punch. Plane waves were observed prior to injury (left), whereas pinned spiral waves were observed following injuries. A single pinned spiral wave resulted from a single hole injury (middle), whereas counter-propagating pinned spirals resulted from the two-hole injury model (right). In all cases, the temporal derivative of calcium intensity is shown and exposure times were 5 msec. Culture day is 12.

Movie S13, Calcium propagation on a neonatal rat ventricular myocyte tissue-engineered ventricle following injury with a 1-mm diameter biopsy punch. A single pinned spiral wave, with rotation rate ~5 Hz, resulted from the single-hole injury. The temporal derivative of calcium intensity is shown and exposure times were 10 msec. Culture day is 12. The model ventricle shown here, is the same one shown in Supplementary Movie S12, using different exposure times during acquisition of the calcium fluorescence signal.

Movie S14, Contraction of neonatal rat ventricular myocyte (NRVM) tissues following 40 days of culture in polycaprolactone-gelatin nanofibrous sheets. Left panels show NRVM tissue (top) and nanofibers (bottom), and the right panel shows a displacement heat map overlying the contractile NRVM tissue. These show NRVM contractile anisotropy guided by the underlying substrate and maintained for extended culture periods.

Movie S15, Membrane staining of neonatal rat ventricular myocyte (NRVM) tissues following 45 days of culture in polycaprolactone-gelatin nanofibrous sheets. Confocal z-stack reconstructions show tissue compaction at the surface, alignment preserved beneath the tissue surface, and early-stage evidence of cardiomyocyte maturation (e.g., cell geometry, staggered membrane junctions and membrane striations).